



Geophysical Research Letters



RESEARCH LETTER

10.1029/2020GL088621

Key Points:

- We ray-trace 3 × 10⁷ satellite gravity wave measurements over the Southern Ocean
- We see evidence of southward wave propagation into a band at ~60°S
- Our evidence suggests that waves from near-surface sources in the Southern Ocean region are a plausible source of "missing" model momentum flux

Supporting Information:

- supporting Information S1
- supporting Information S2
- supporting Information S3
- supporting Information S4

Correspondence to:

C. J. Wright, c.wright@bath.ac.uk

Citation:

Perrett, J. A., Wright, C. J., Hindley, N. P., Hoffmann, L., Mitchell, N. J., Preusse, P., et al. (2021). Determining gravity wave sources and propagation in the Southern Hemisphere by ray-tracing AIRS measurements. *Geophysical Research Letters*, 48, e2020GL088621. https://doi.org/10.1029/2020GL088621

Received 4 MAY 2020 Accepted 14 DEC 2020

© 2020. The Authors.

This is an open access article under the terms of the Creative Commons Attribution License, which permits use, distribution and reproduction in any medium, provided the original work is properly cited.

Determining Gravity Wave Sources and Propagation in the Southern Hemisphere by Ray-Tracing AIRS Measurements

Jon A. Perrett¹, Corwin J. Wright¹, Neil P. Hindley¹, Lars Hoffmann², Nicholas J. Mitchell¹, Peter Preusse³, Cornelia Strube³, and Stephen D. Eckermann⁴

¹Centre for Space, Atmospheric and Oceanic Science, University of Bath, Bath, UK, ²Jülich Supercomputing Centre, Forschungszentrum Jülich, Jülich, Germany, ³Institute of Energy and Climate Research—Stratosphere, Forschungszentrum Jülich, Jülich, Germany, ⁴Space Science Division, U.S. Naval Research Laboratory, Washington, DC, USA

Abstract Gravity waves (GWs) are key drivers of atmospheric circulation. Understanding their sources and propagation is essential to improving weather and climate models. We apply a 3D Stockwell Transform to 1 month of stratospheric temperature data from NASA's Atmospheric InfraRed Sounder to obtain 3D GW measurements and parameters. We use ray-tracing methods to determine the sources and propagation characteristics of these GWs over the entire Southern Ocean. We trace 1.28 million GW measurements per day for the month of June 2010. Our analysis suggests that ground-based sources around the Andes, Antarctic Peninsula, and Kerguelen play major roles, and that the GWs generated by these and other sources travel large zonal distances. We show evidence that GWs propagate into the 60°S belt, a possible source of "missing momentum flux" in GCMs at this latitude. These results emphasize the need for models to incorporate the possibility that GWs can exhibit large horizontal propagation.

Plain Language Summary Gravity waves are atmospheric waves that transport large amounts of energy through the atmosphere. Understanding their sources and propagation characteristics is key to improving climate models. We trace 30 million wave measurements back to their sources over the Southern Ocean. We find that wave sources in this region are mainly small, mountainous islands and the Andes mountain range, a well-known gravity wave "hot spot." These waves propagate southwards, a feature that is not implemented in many climate models. Hence, the momentum carried by the gravity waves is deposited at the wrong place in these models. We also find that waves travel many hundreds of kilometers west to east. This evidence suggests that atmospheric models need to improve their handling of gravity waves, and more accurately model the way they travel.

1. Introduction

Gravity waves (GWs) are key drivers of the atmospheric general circulation. They transport a significant fraction of the momentum needed to constrain the atmospheric mean flow above the troposphere. GWs are generated by a complex mix of sources primarily located at surface and lower-atmospheric levels (e.g., Fritts & Alexander, 2003, and references therein).

One of the most intense regions of GW activity is the stratosphere above the Southern Ocean in austral winter (e.g., Hindley et al., 2015, and references therein). Despite the known importance of GWs to the dynamics of this region, weather and climate models are known to consistently underestimate GW momentum fluxes here. This leads to significant biases in the simulated large-scale circulation (e.g., Garcia et al., 2017; McLandress et al., 2012). Therefore, understanding the sources and propagation characteristics of GWs is vitally important to improving our understanding and simulations of the Antarctic high-latitude circulation, which in turn impacts upon weather, ozone and climate processes at both local and global scales (e.g., Garcia et al., 2017; Hansen & Chipperfield, 1999; Lim et al., 2019).

Previous work has clearly and consistently shown evidence of strong stratospheric GW activity located over the Andes, Antarctic Peninsula and small mountainous islands in the open Southern Ocean (e.g., Alexander & Grimsdell, 2013; Eckermann & Preusse, 1999; Geller et al., 2013; Hindley et al., 2015; Hoffmann

PERRETT ET AL. 1 of 10



et al., 2016). In general circulation models, these waves are assumed propagate near-vertically upwards in a model column; the GW activity routinely seen above these features is directly consistent with these assumptions. However, a significant "tail" of GWs, starting at the Andes and extending in an eastward direction almost the entire distance around the Earth (e.g., Hindley et al., 2015), has proven much more challenging to explain.

One approach to investigate the origin of this tail is to use ray-tracing. In ray-tracing, a GW with an initial set of properties is propagated either forwards or backwards in time through background wind and stability fields. Assuming that the initial parameters are chosen well and that the wind fields are accurate, backwards-traced rays should pass through the source of the wave, while forwards-traced waves show the path they take from the initial time point onwards. For early studies (e.g., Eckermann & Marks, 1996; Zhong et al., 1995), wind fields were usually coarse in resolution and the GW properties estimated from theory, but with modern reanalyses more accurate wind fields can be used, and more accurate initial parameters can now be estimated from observations.

Consequently, several previous studies have used a ray-tracing approach to understand the sources and propagation characteristics of GWs over all or part of the Southern Ocean. These studies have used GW parameters and background fields sourced in various ways. Common approaches have included idealized and/or isotropic GW source spectra (Preusse et al., 2006, 2009; Wells et al., 2011) or the estimation of the necessary GW parameters from model or reanalysis output (Jiang et al., 2013; Preusse et al., 2014; Sato et al., 2012; Vosper, 2015), and propagated those GWs through model or reanalysis wind fields. A less common approach has been the use of observationally derived parameters; (e.g., Pulido et al., 2013), who backwards-traced radiosonde-derived GW parameters from an Argentina-based launch campaign through winds estimated from a high-resolution WRF model simulation over the Andes. Combined, these idealized, model-based and observationally based studies suggest that (i) the downstream propagation of GWs from the Andes is proportional to their horizontal wavelength (Wells et al., 2011), (ii) that waves in this region typically propagate southwards or southeastwards into the polar jet at around 60°S (Ehard et al., 2017; Jiang et al., 2013; Sato et al., 2012; Vosper, 2015) and (iii) that many of these waves have orographic sources (Pulido et al., 2013).

This body of previous work exhibits some limitations, which the present study addresses. One key limitation is spatial coverage of the GW observations. Due to the significant computational cost of such studies and/or limited GW parametric information, almost all of the above works focus on specific limited areas, such as around small islands (Vosper, 2015) and the Andes and Antarctic Peninsula (Pulido et al., 2013; Sato et al., 2012). Studies which do cover large areas (e.g., Preusse et al., 2014) have used model-derived or idealized GW parameters. Key questions therefore remain about whether the conclusions of this earlier work (i) reflect the observed properties of real GWs and (ii) accurately describe GW propagation across the entirety of this large and important region.

Accordingly, we here for the first time ray-trace observed GWs over the entire Southern Ocean region. We measure the GWs and the parameters needed to ray-trace them using satellite data from NASA's Atmospheric InfraRed Sounder (AIRS), then apply the Gravity Wave Regional Or Global Ray Tracer (GROGRAT) ray-tracer to these parameters to trace the waves back to their origins (Eckermann & Marks, 1996; Marks & Eckermann, 1995). We derive our wind fields from the ERA5 reanalysis, which is observationally well-constrained at large scales in this region (Wright & Hindley, 2018) to provide suitable accuracy for this task. We trace over 30 million measurements taken at a height of about 40 km altitude back to their sources, which we believe represents the largest observationally based GW ray-tracing study ever performed.

Section 2 describes the datasets used, and Section 3 the GW detection methods and basic concepts underlying GROGRAT. We then describe the GW measurements made and the results of ray-tracing these GWs in Section 4, before drawing conclusions in Section 5.

2. Data

2.1. AIRS

The Atmospheric InfraRed Sounder (AIRS) is a nadir-sounding hyperspectral imager on NASA's Aqua satellite, part of the A-Train sun-synchronous constellation. AIRS scans a \pm 49° swath either side of the orbital

PERRETT ET AL. 2 of 10



track (Aumann et al., 2003). This swath is processed into 90 across-track elements, with a horizontal resolution of 13.5 km at swath center falling to \sim 41 km at swath edge. The data are stored every 6 min as a "granule" of 135 consecutive along-track elements, producing 240 granules of 90 \times 135 elements per day.

We use data generated using the AIRS L2 retrieval of Hoffmann and Alexander (2009); this produces temperature data at the full horizontal resolution of the instrument on a 3 km vertical grid throughout the stratosphere. Retrieval error and noise are lowest in the altitude range 20–60 km (Hindley et al., 2019; Hoffmann & Alexander, 2009), so we only consider these data. In this range, retrieval error in the temperature measurements is 1.6–3.0 K, and vertical resolution varies between 7 and 15 km (Hindley et al., 2019). AIRS data are sensitive only to a portion of the GW spectrum with horizontal wavelengths less than 1,400 km and vertical wavelengths larger than 15 km (Ern et al., 2017). GWs in this spectral regime contribute heavily to total GWMF (Ern et al., 2004; Meyer et al., 2018), and thus although we are seeing only a subset of the GW spectrum, it is a subset with a significant impact on atmospheric dynamics.

2.2. ERA-5

ERA-5 is the most recent reanalysis produced by the European Center for Medium-range Weather Forecasting (ECMWF) (Ehard et al., 2018; Hersbach et al., 2020). We use ERA-5 temperatures and zonal and meridional wind reanalysis fields, at a $1.5 \times 1.5^{\circ}$ (latitude \times longitude) resolution on 137 levels from the surface to 0.01 hPa at a 3 h time resolution. We vertically interpolate these global fields to a regular 1 km spacing from the surface to 75 km altitude. We further smooth the fields using a $(7 \times 7 \times 7)$ -voxel boxcar in space; this is intended to remove the impact of localized temperature gradients in the background field caused by gravity waves which are directly resolved on the reanalysis grid but which may not match those in our satellite observations.

3. Methods

3.1. Obtaining Wave Properties—The 3D Stockwell Transform and AIRS

To provide the information needed to ray-trace measured GWs, we must both estimate their physical parameters and spatially localize where they occur. We therefore require a spectral analysis technique that localizes the wave event in both spectral and position space. We here use the Stockwell Transform (S-Transform) (Stockwell et al., 1996), which has been widely used in previous studies (Alexander et al., 2010; Hindley et al., 2016; Wright et al., 2017; Wright & Gille, 2013).

We first interpolate T' to a regular distance grid. Following Wright et al. (2017), we then remove the exponential increase of wave amplitude with height, based at a reference point at 39 km altitude, as $exp((z-z_0)/2H)$. This compensates for the dominating effect of larger amplitudes at the higher altitudes of the granule on the S-Transform, and is reversed in a later step in order to ensure no net effect on measured amplitudes. We then detrend the data with a fourth-order cross-track polynomial filter independently for each height level and along-track row, consistent with previous studies using AIRS. This produces estimates of temperatures perturbations T', which include systematic perturbations due to GWs, and of the smoothly varying background temperature \overline{T} . We also apply a horizontal 3×3 voxel boxcar smoother in the horizontal plane, to reduce the effects of small-scale noise in the AIRS data. The horizontal wavelengths measured from this method range from 40 km to around 1,000 km (Hindley et al., 2019).

We next apply the 3D S-Transform to the temperature perturbation data. This produces a 6D output $S(\tau, \mathbf{f}) = S((\mathbf{X}), \mathbf{f}) = S(x, y, z, f_x, f_y, f_z)$, where $f_{x,y,z}$ are spatial frequencies (inverse of wavelength) in the x, y, z directions, respectively. Following Hindley et al. (2016), we reduce this 6D field to several 3D fields. First, for each location in \mathbf{x} , we determine the single wave with the largest spectral amplitude, giving us a complex object $\mathcal{A}(\mathbf{x})$. The locations of $\mathcal{A}(\mathbf{x})$ within $S((\mathbf{X}), \mathbf{f})$ correspond to the wavenumbers of the dominant wave at each \mathbf{x} . This gives us $\mathcal{F}_x(\mathbf{x}), \mathcal{F}_y(\mathbf{x}), \mathcal{F}_z(\mathbf{x})$, corresponding to the f_x, f_y, f_z frequencies that are dominant at each location in \mathbf{x} . These four 3D fields are the same size as the input data $h(\mathbf{x})$.

Using the cross-track and along-track azimuths at each point on the granule, we then in local geophysical coordinates project the components of the spatial frequencies into the three-dimensional spatial wave

PERRETT ET AL. 3 of 10



vector (inverse of frequency) (k, l, m), and use the magnitude of \mathcal{A} to obtain the amplitude, from which we remove the scaling applied above. As the AIRS granule is just a single snapshot in time, there is a 180° ambiguity about the propagation direction of measured gravity waves. To break this ambiguity, we assume that all gravity waves measured are upwardly propagating (Ern et al., 2017; Wright et al., 2016, 2017), by requiring m to be negative. After directly fitting these parameters from the S-Transform, we compute estimates of wave phase speed and temporal frequency from the spectral data, following the method of Wright et al. (2017).

3.2. Ray-Tracing of Gravity Waves—GROGRAT

To ray-trace, we use GROGRAT. Initial GW parameters are obtained as described above, and background meteorological fields are obtained from ERA-5. Introduced by Marks and Eckermann (1995), GROGRAT is a GW ray-tracer based on the dispersion relation

$$\hat{\omega}^2 = (\omega - Uk - Vl)^2 = \frac{N^2 (k^2 + l^2) + f^2 (m^2 + \alpha^2)}{k^2 + l^2 + m^2 + \alpha^2},$$
(1)

where U and V are zonal and meridional wind, $\hat{\omega}$ is the GW intrinsic frequency (i.e., the frequency an observer moving with the background wind would observe), ω is the ground-based frequency, N is the Brunt-Väisälä (buoyancy) frequency, f is the Coriolis parameter, f is the GW wavenumber vector, and f is f where f is the atmospheric scale height (assumed to be 7 km).

The ray-tracing equations used in GROGRAT are derived by Lighthill (1967). The position of the ray and refraction of the wavevector along the ray in time, respectively, are computed as:

$$\frac{dx_i}{dt} = \frac{\partial \omega}{\partial k_i} \quad \text{and} \quad \frac{dk_i}{dt} = -\frac{\partial \omega}{\partial x_i}$$
 (2)

Via the dispersion relation, solving these equations is based on U, V, and N background values, which we estimate using ERA-5. The version of GROGRAT used in this study also implements the spherical geometry corrections derived by Hasha et al. (2008), allowing rays to travel along great circles. This is especially important for rays traveling large horizontal distances or close to the poles. The time step dt is modulated throughout the trace to select the longest time step which produces an error below a threshold of 1%, striking a balance between computational speed and accuracy.

We backwards-trace our rays from observation to origin, but it is important to note that the source of the GW could be anywhere along the path rather than where the ray is calculated to terminate by GROGRAT (Preusse et al., 2014). To increase our certainty about the origins of our rays, we examine derived GW phase speeds and frequencies alongside measured wavelengths in combination with the inferred raypaths to better contextualize possible sources.

For the month of June 2010, we backward-trace all AIRS data in the Southern Hemisphere, from the layer of voxels at 39 km downwards toward their origins. This is at the center of our vertical measurement range, allowing us to measure long vertical wavelengths that would not be accessible to the S-Transform technique at lower or higher altitudes due to edge-truncation effects. For each voxel with a measured temperature perturbation $\hat{T} > 1.5 \mathrm{K}$, we use the 3DST to measure the wave's initial position, 2D horizontal wavenumber (k, l), ground-based frequency ω via (1), and horizontal wind amplitude \hat{u}_{\parallel} , which we compute (Hu et al., 2002) as

$$\frac{\hat{T}}{\overline{T}} = \left[im + 1/(2H)\right] \frac{\hat{\omega}^2 - f^2}{g\hat{\omega}\sqrt{k^2 + l^2}} \cdot \hat{u}_{\parallel}.$$
 (3)

For each granule, we can trace a maximum of $90 \times 135 = 12{,}150$ individual measurements. On average after allowing for the above amplitude filtering, we actually trace paths from 1.28 million voxels per day.

PERRETT ET AL. 4 of 10

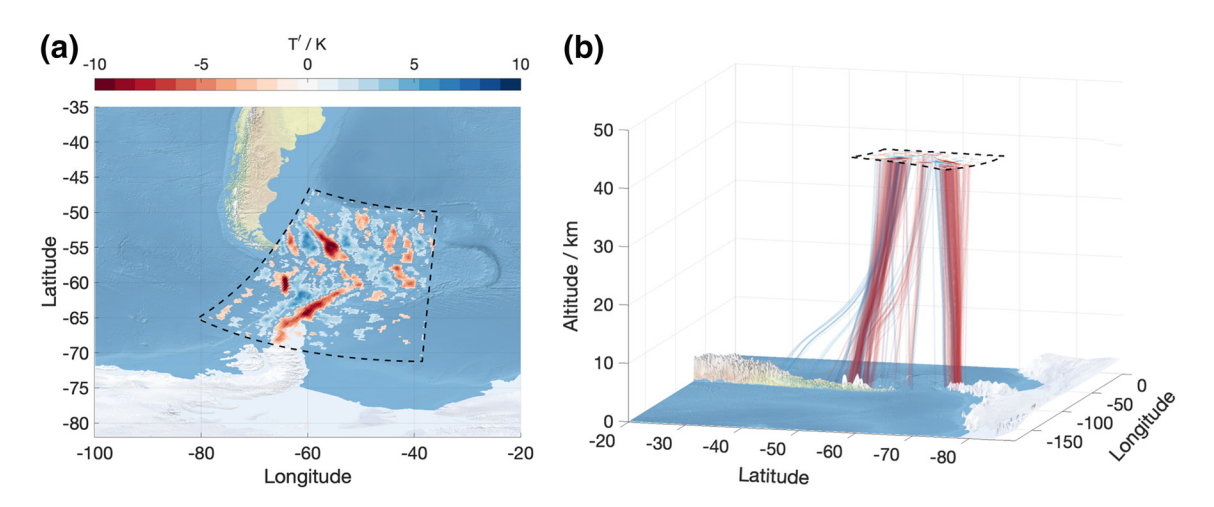


Figure 1. An AIRS granule measured on 4 June 2010 at around 04:10 UTC over the Drake Passage ray-traced back to its source. (a) GW temperature perturbations at 39 km altitude as seen by the AIRS temperature retrievals (values less than 1.5 K are not colored). (b) Ray-tracing paths from the voxels at 39 km in this granule. Colors correspond to the source voxels *T'*, shown in Figure 1a). AIRS, Atmospheric InfraRed Sounder; GC, gravity waves.

4. Results

4.1. Case Study over Southern Andes

Figure 1 demonstrates the raypaths generated from tracing a single AIRS granule observed near the Drake Passage, measured on June 4, 2010 at around 04:10 UTC. GW T' at 39 km is shown in Figure 1a. We see a chevron-like pattern, indicative of potential GW sources in both the Antarctic Peninsula and Southern Andes. Figure 1b shows rays produced by ray-tracing each voxel in this 39 km layer backwards in time. We see rays from the northern half of the granule terminating near the surface around the Andes, and rays from the southern half of the granule terminating around the Antarctic Peninsula. This hence demonstrates simultaneous northward propagation of GWs from the Antarctic Peninsula and southward propagation of GWs from the Andes into the Drake Passage region. This has been previously been theoretically demonstrated by Sato et al. (2012), using idealized background wind and initial GW parameters. We obtain a similar height of convergence as Sato et al. (2012), who saw this occurring at \sim 40 km altitude. The raypaths become increasingly vertical with height, as has previously been seen using 3D group velocity measurements over the Andes by Wright et al. (2017).

Using simulated GWs in a high-resolution model, Sato et al. (2012) also suggested that GWs over the Andes with horizontal wavenumber angles around 220° will propagate roughly 10° in longitude from the Andes by the time they reach 40 km. For the northern portion of this granule over the Andes, we measure a horizontal wavenumber angle of 215°, anticlockwise from east. We see similar propagation characteristics as Sato et al. (2012) in this case study.

4.2. Ray-Tracing Over the Southern Ocean—June 2010

Building upon the case study of section 4.1, we proceed to ray-trace all AIRS granules over the Southern Ocean in June 2010. This month was chosen as the wave activity was strongest for 2010 austral winter (Hindley et al., 2019). This allows us to examine GW sources and propagation characteristics over the entire region. We again note that we are inferring GW sources from a combination of AIRS derived GW phase speeds and frequencies, AIRS measured wavelengths and the characteristics of the raypaths.

Figure S2 shows the distribution of mean ray launch and termination points. The much denser regions over the Antarctic continent are due to a much greater number of overpasses being averaged, due to the polar orbit of AIRS. As this region is in near constant darkness, there are also many more observations included in our average per satellite overpass.

We first present the 3DST-derived GW parameters used as input for the ray-tracing analysis. These are shown in Figure 2. Data are shown as the monthly mean of all voxels, on a $1.5 \times 1.5^{\circ}$ grid. Voxels with an

PERRETT ET AL. 5 of 10

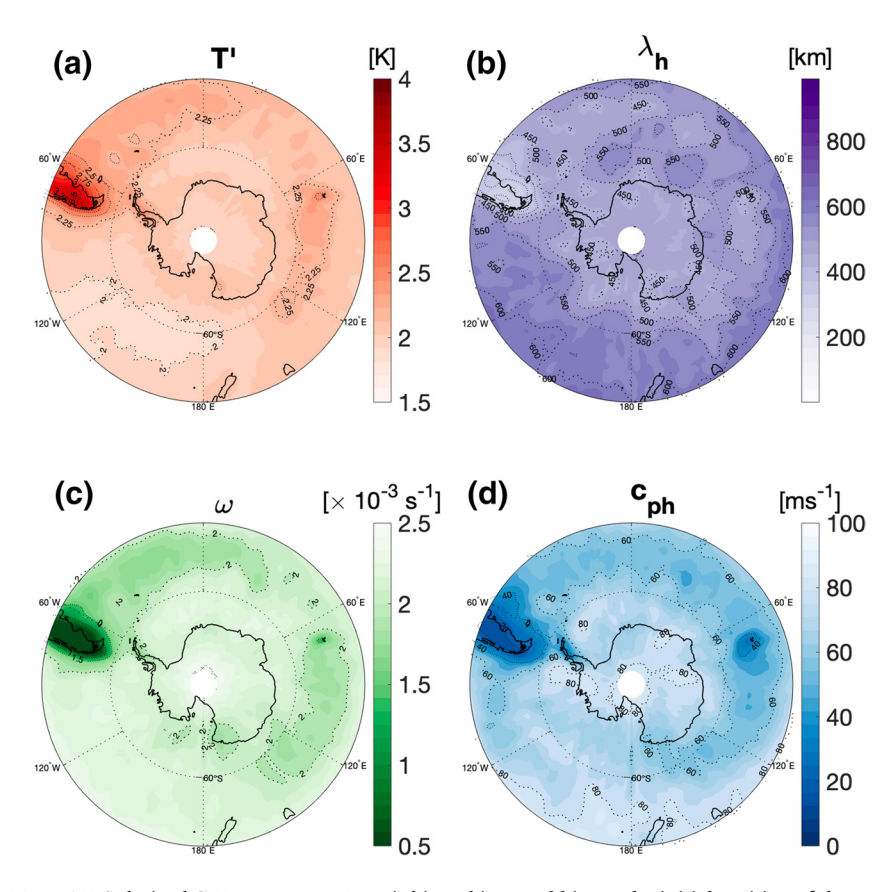


Figure 2. Mean AIRS-derived GW parameters. Data is binned into 1.5° bins at the initial position of the ray-tracing at 39 km. (a) Temperature amplitude of the wave/ (k) (b) horizontal wavelength/km⁻¹, (c) ground-based frequency/s⁻¹, (d) Ground-based phase speed/m s⁻¹. AIRS, Atmospheric InfraRed Sounder; GW, gravity waves.

amplitude less than 1.5 K have been removed from all variables before both plotting and ray-tracing, consistent with the instrument noise analysis presented in Figure 2 of Hindley et al. (2019). We also remove all data poleward of 85°S, as Wright and Hindley (2018) showed very low correlation (r < 0.4) between ERA5 and satellite temperature observations at the initial 39 km height this close to the pole. Since ray-tracing relies on the accuracy of the background fields, using data from this region may provide results much less reliable than for other regions.

Figure 2a shows average temperature amplitudes. Note that these temperature amplitudes are converted to wind amplitudes before the ray-tracing analysis; however, we show the temperature amplitudes here since they are the measured quantity. We see a primary peak over the southern Andes and Antarctic Peninsula, extending $\sim 80^{\circ}$ downstream to the east. We also see a secondary maximum over Kerguelen (49°S, 69°E), extending $\sim 60^{\circ}$ eastwards. There is also some evidence of increased activity relative to the surrounding region over South Georgia (54°S, 36°W) and New Zealand; however, both maxima represent only a small increase above the background, and the maximum from South Georgia in particular is hard to distinguish due to the long tail of Andean and Antarctic Peninsula activity.

Figure 2b) shows initial horizontal wavelengths $\lambda_h = (\sqrt{k^2 + l^2})^{-1}$. This map shares some features with Figure 2a, but also exhibits some key differences. We see minima over the Andes and Kerguelen, similar to Hindley et al. (2019). We also see longer wavelengths over the open ocean, with smaller wavelengths occurring over topography. We observe some indication of an inward spiral of shorter wavelengths over the Southern Ocean starting at the Andes and passing over Kerguelen into the Admiralty Mountains, as seen by previous studies (e.g., Hendricks et al., 2014; Hindley et al., 2019, 2015; McLandress et al., 2012; Sato et al., 2012).

Finally, Figures 2c and 2d show ground-based frequency and ground-based horizontal phase speed; note that the color scale in these figures is reversed relative to Figures 2a and 2b. These variables are both derived

PERRETT ET AL. 6 of 10

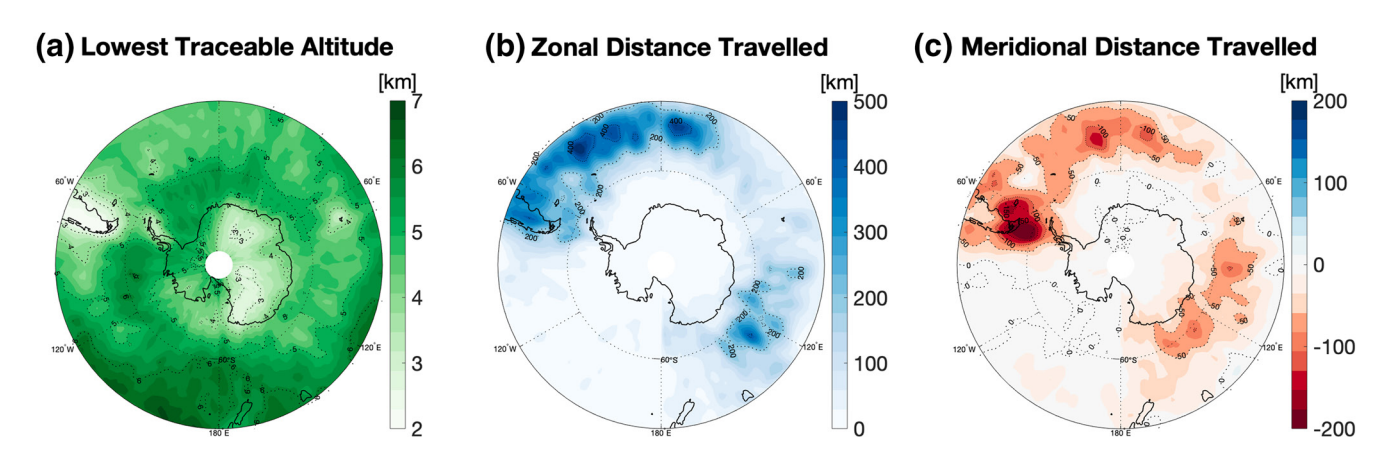


Figure 3. Ray derived characteristics from June 2010 AIRS data over the Southern Ocean. Data is in $1.5 \times 1.5^{\circ}$ bins. (a) Lowest Traceable Altitude (The lowest altitude raypaths reach before termination), binned by termination location. (b) Zonal (Eastward) distance traveled from lowest traceable altitude to measurement point at 39 km, binned by measurement location. (c) Meridional (Northward) distance traveled from lowest traceable altitude to measurement point at 39 km, binned by measurement location. AIRS, Atmospheric InfraRed Sounder.

from measured properties using linear GW theory (Fritts & Alexander, 2003; Wright et al., 2017). The values here are consistent with Figures 2a and 2b, with a region of particularly low frequency consistent with orographic generation over the southern Andes. Although for a different year, these values agree quantitatively with Wright et al. (2017). We more clearly see the spiral feature described by previous work, particularly in Figure 2d and, with a secondary minimum over Kerguelen. In Figure 2d, we see regions of lower ($<30 \text{ m s}^{-1}$) phase speed around the southern Andes, Antarctic Peninsula, South Georgia and the Kerguelen Islands, indicative of orographic GW activity. For true orographic generation, measured phase speeds over these regions would be zero; this difference is likely due to the combined effects of nonorographic GWs from storms and jets being included in our averages (Hoffmann et al., 2016; Preusse et al., 2014), and measurement uncertainties propagating through the calculation (Wright et al., 2017).

4.3. GW Sources and Propagation Characteristics through Ray-Tracing

Figure 3a shows the monthly mean Lowest Traceable Altitude (LTA) reached by each ray, averaged on a $1.5 \times 1.5^{\circ}$ grid. This is the lowest altitude the raypath reaches when back-tracing, before being terminated by GROGRAT due to either reaching the ground or entering an atmospheric regime where the wave cannot be physically supported. Data shown here have been geolocated at the termination point of the ray. We see distinct regions of low LTA around the southern Andes, the Antarctic Peninsula, and Kerguelen, where the mean LTA is <4 km, and less than <2 km for the Andes. There is also a small region of sub-4 km altitude LTA near South Georgia; this is the only other location to have an LTA this low. These LTA-minima are indicative of GW sources in these regions originating near to or at the surface, averaged together with other nonsurface sources. A similar analysis by Preusse et al. (2014) demonstrated regions of low LTA over the Andes and Antarctic Peninsula, however these were much less localized, and did not display the clear sources over small mountainous islands we see in Figure 3a.

There are also regions of low LTA over the Antarctic continent. However, when considered in the context of the high phase speeds seen over these regions (Figure 2d, it is less probable that these waves are orographic in origin. When we consider the higher phase speeds measured in this region and the small distances traveled (Figures 3b and 3c), this suggests that this could be due to GWs originating from near-surface nonorographic sources.

However, low LTAs over Antarctica have also been seen by Mehta et al. (2017), with higher phase speed measurements originating near the surface around the south pole. Preusse et al. (2014) also observed regions of low LTA over the south pole, possibly due to Katabatic winds.

Figure 3b shows the average zonal distance traveled by raypaths from their LTA to their measurement point at 39 km, geolocated at their 39 km measurement location. This provides information on how

PERRETT ET AL. 7 of 10



geographically local GW sources are to where the waves are measured in the midstratosphere. Comparing to Figure 2b, we see a positive correlation between horizontal wavelength and zonal propagation, agreeing with previous studies (Wells et al., 2011). We see two patches where GWs have on average traveled large zonal distances.

Over Kerguelen, the zonal distance traveled is close to zero, indicative of orographic waves generated in this region that are ascending vertically upwards through the atmosphere.

In contrast, higher zonal distances are seen for GWs originating over the Andes. The underlying cause of this effect is demonstrated in Figure 1: examination of the direct ray-traces (omitted for brevity) shows that many rays in this region travel long horizontal distances in the troposphere and lower stratosphere before traveling vertically upwards toward their measurement altitude, rather than directly upwards over the Andes.

All GW traces move eastward in the Southern Hemisphere (Figure S3). In austral winter, the Southern Ocean is known for strong, westerly winds, regularly exceeding 60–80 m s⁻¹ in the stratosphere (Figure S1); therefore, under our initial assumption that measured GWs are upwardly propagating, this is consistent with the waves being refracted by these strong, westerly winds as they travel from their lowest point to the measurement altitude.

Figure 3c shows that GWs measured in the patches of larger GW activity propagate southwards, converging around 60°S, south of which they are replaced by waves which have on average traveled only very short distances both zonally and meridionally with high LTAs. Previous studies have implied this result through measurements of converging wave direction at this latitude, both in observations and models (Hindley et al., 2019; Holt et al., 2017; Sato et al., 2012). Propagation of GWs into this region is hypothesized to be one of the key reasons global climate models underestimate momentum flux around the Southern Ocean (Hindley et al., 2015, 2019; McLandress et al., 2012), and thus this further demonstrates the need for climate models to model meridional propagation of gravity waves.

5. Conclusion

We have performed what we believe to be the largest-ever backwards ray-tracing study of measured atmospheric gravity waves, focusing on the region above the Southern Ocean and Antarctica. Building upon previous work, we backwards-trace GW rays from mid-stratospheric measurements to the lower atmosphere, allowing us to determine their likely sources. We show clear evidence for significant surface GW sources around the Andes, Antarctic Peninsula and Kerguelen. In comparison with previous ray-tracing studies, we see much finer localization of sources, especially over orography.

In ray-tracing the waves backwards, we find that the GWs observed by AIRS often travel many hundreds of kilometers zonally from their source location. Since many of these waves will be unresolved in climate models, this suggests that the standard assumption in GW parameterization that subgrid scale GWs travel with no significant horizontal propagation is a poor approximation in this region. Our results clearly demonstrate the need for improvements in these schemes which will allow subgridscale GWs to propagate in a more realistic manner.

We also show that GWs around the Southern Ocean region propagate into and converge around a belt at 60°S. This builds on previous studies, providing further clear evidence that this convergence happens all around the region. Missing propagation of GWs into this belt is hypothesized to be one of the key reasons global climate models underestimate momentum flux around the Southern Ocean.

Data Availability Statement

AIRS data used in this study were originally obtained from NASA's DISC service, and have been preprocessed as described in Hoffmann and Alexander (2009), and are available from https://datapub.fz-juelich.de/slcs/airs/gravity_waves/data/jon/. ERA5 data were downloaded from the Copernicus Climate Change

PERRETT ET AL. 8 of 10



Service Climate Data Store: https://cds.climate.copernicus.eu/. This research made use of the Balena High Performance Computing (HPC) Service at the University of Bath.

Acknowledgments

J. A. Perrett is funded by Royal Society grant RGF/EA/180217. C. J. Wright is funded by Royal Society grant UF160545 and NERC grant NE/ S00985X/1. C. J Wright, N. P. Hindley, and N. J Mitchell are funded by NERC grant NE/R001391/1. S. D. Eckermann's research was supported by the Chief of Naval Research.

References

- Alexander, M. J., Geller, M., McLandress, C., Polavarapu, S., Preusse, P., Sassi, F., et al. (2010). Recent developments in gravity-wave effects in climate models and the global distribution of gravity-wave momentum flux from observations and models. *Quarterly Journal of the Royal Meteorological Society*, 136(650), 1103–1124.
- Alexander, M. J., & Grimsdell, A. W. (2013). Seasonal cycle of orographic gravity wave occurrence above small islands in the southern hemisphere: Implications for effects on the general circulation. *Journal of Geophysical Research: Atmospheres*, 118,11589–11599. https://doi.org/10.1002/2013JD020526
- Aumann, H., Chahine, M., Gautier, C., Goldberg, M., Kalnay, E., McMillin, L., et al. (2003). AIRS/AMSU/HSB on the aqua mission: Design, science objectives, data products, and processing systems. *IEEE Transactions on Geoscience and Remote Sensing*, 41(2), 253–264.
- Eckermann, S. D., & Marks, C. J. (1996). An idealized ray model of gravity wave-tidal interactions. *Journal of Geophysical Research*, 101(D16), 21195–21212. https://doi.org/10.1029/96jd01660
- Eckermann, S. D., & Preusse, P. (1999). Global measurements of stratospheric mountain waves from space. Science, 286(5444), 1534–1537. https://doi.org/10.1126/science.286.5444.1534
- Ehard, B., Kaifler, B., Dörnbrack, A., Preusse, P., Eckermann, S. D., Bramberger, M., et al. (2017). Horizontal propagation of large-amplitude mountain waves into the polar night jet. *Journal of Geophysical Research: Atmospheres*, 122, 1423–1436. https://doi.org/10.1002/2016JD025621
- Ehard, B., Malardel, S., Dörnbrack, A., Kaifler, B., Kaifler, N., & Wedi, N. (2018). Comparing ECMWF high-resolution analyses with lidar temperature measurements in the middle atmosphere. *Quarterly Journal of the Royal Meteorological Society*, 144(712), 633–640. https://doi.org/10.1002/gi.3206
- Ern, M., Hoffmann, L., & Preusse, P. (2017). Directional gravity wave momentum fluxes in the stratosphere derived from high-resolution AIRS temperature data. *Geophysical Research Letters*, 44, 475–485. https://doi.org/10.1002/2016GL072007
- Ern, M., Preusse, P., Alexander, M. J., & Warner, C. D. (2004). Absolute values of gravity wave momentum flux derived from satellite data. Journal of Geophysical Research, 109, D20103. https://doi.org/10.1029/2004JD004752
- Fritts, D. C., & Alexander, M. J. (2003). Gravity wave dynamics and effects in the middle atmosphere. *Reviews of Geophysics*, 41(1), 1–64. Garcia, R. R., Smith, A. K., Kinnison, D. E., de la Cámara, Á., & Murphy, D. J. (2017). Modification of the gravity wave parameterization in the whole atmosphere community climate model: Motivation and results. *Journal of the Atmospheric Sciences*, 74(1), 275–291. https://doi.org/10.1175/jas-d-16-0104.1
- Geller, M. A., Alexander, M. J., Love, P. T., Bacmeister, J., Ern, M., Hertzog, A., et al. A comparison between gravity wave momentum fluxes in observations and climate models. *Journal of Climate*, 26(17), 6383–6405. https://doi.org/10.1175/jcli-d-12-00545.1
- Hansen, G., & Chipperfield, M. P. (1999). Ozone depletion at the edge of the arctic polar vortex 1996/1997. *Journal of Geophysical Research*, 104(D1), 1837–1845. https://doi.org/10.1029/1998jd100021
- Hasha, A., Bühler, O., & Scinocca, J. (2008). Gravity wave refraction by three-dimensionally varying winds and the global transport of angular momentum. *Journal of the Atmospheric Sciences*, 65(9), 2892–2906.
- Hendricks, E. A., Doyle, J. D., Eckermann, S. D., Jiang, Q., & Reinecke, P. A. (2014). What is the source of the stratospheric gravity wave belt in austral winter?. *Journal of the Atmospheric Sciences*, 71(5), 1583–1592.
- Hersbach, H., Bell, B., Berrisford, P., Hirahara, S., Horányi, A., Muñoz-Sabater, J., et al. (2020). The ERA5 global reanalysis. *Quarterly Journal of the Royal Meteorological Society*, 146(730), 1999–2049. https://doi.org/10.1002/qj.3803
- Hindley, N. P., Smith, N. D., Wright, C. J., Rees, D. A. S., & Mitchell, N. J. (2016). A two-dimensional stockwell transform for gravity wave analysis of AIRS measurements. *Atmospheric Measurement Techniques*, 9(6), 2545–2565.
- Hindley, N. P., Wright, C. J., Smith, N. D., Hoffmann, L., Holt, L. A., Alexander, M. J., et al. (2019). Gravity waves in the winter stratosphere over the southern ocean: High-resolution satellite observations and 3-d spectral analysis. Atmospheric Chemistry and Physics Discussions, 19, 15377–15414.
- Hindley, N. P., Wright, C. J., Smith, N. D., & Mitchell, N. J. (2015). The southern stratospheric gravity wave hot spot: Individual waves and their momentum fluxes measured by cosmic gps-ro. *Atmospheric Chemistry and Physics*, 15(14), 7797–7818. https://doi.org/10.5194/
- Hoffmann, L., & Alexander, M. J. (2009). Retrieval of stratospheric temperatures from atmospheric infrared sounder radiance measurements for gravity wave studies. *Journal of Geophysical Research*, 114, D07105. https://doi.org/10.1029/2008JD011241
- Hoffmann, L., Grimsdell, A. W., & Alexander, M. J. (2016). Stratospheric gravity waves at southern hemisphere orographic hotspots: 2003–2014 airs/aqua observations. Atmospheric Chemistry and Physics, 16(14), 9381–9397. https://doi.org/10.5194/acp-16-9381-2016
- Holt, L. A., Alexander, M. J., Coy, L., Liu, C., Molod, A., Putman, W., & Pawson, S. (2017). An evaluation of gravity waves and gravity wave sources in the southern hemisphere in a 7 km global climate simulation. *Quarterly Journal of the Royal Meteorological Society*, 143(707), 2481–2495. https://doi.org/10.1002/qj.3101
- Hu, X., Liu, A. Z., Gardner, C. S., & Swenson, G. R. (2002). Characteristics of quasi-monochromatic gravity waves observed with na lidar in the mesopause region at starfire optical range, NM. *Geophysical Research Letters*, 29(24), 2169. https://doi.org/10.1029/2002gl014975
- Jiang, Q., Doyle, J. D., Reinecke, A., Smith, R. B., & Eckermann, S. D. (2013). A modeling study of stratospheric waves over the southern andes and drake passage. *Journal of the Atmospheric Sciences*, 70, 1688–1689.
- Lighthill, M. J. (1967). Waves in fluids. Communications on Pure and Applied Mathematics, 20(2), 267–293.
- Lim, E.-P., Hendon, H. H., Boschat, G., Hudson, D., Thompson, D. W. J., Dowdy, A. J., & Arblaster, J. M. (2019). Australian hot and dry extremes induced by weakenings of the stratospheric polar vortex. *Nature Geoscience*, 12(11), 896–901. https://doi.org/10.1038/ s41561-019-0456-x
- Marks, C. J., & Eckermann, S. D. (1995). A three-dimensional nonhydrostatic ray-tracing model for gravity waves: Formulation and preliminary results for the middle atmosphere. *Journal of the Atmospheric Sciences*, 52(11), 1959–1984.
- McLandress, C., Shepherd, T. G., Polavarapu, S., & Beagley, S. R. (2012). Is missing orographic gravity wave drag near 60s the cause of the stratospheric zonal wind biases in chemistry-climate models?. *Journal of the Atmospheric Sciences*, 69(3), 802–818.
- Mehta, D., Gerrard, A. J., Ebihara, Y., Weatherwax, A. T., & Lanzerotti, L. J. (2017). Short-period mesospheric gravity waves and their sources at the south pole. *Atmospheric Chemistry and Physics*, 17(2), 911–919.

PERRETT ET AL. 9 of 10



- Meyer, C. I., Ern, M., Hoffmann, L., Trinh, Q. T., & Alexander, M. J. (2018). Intercomparison of AIRS and HIRDLS stratospheric gravity wave observations. *Atmospheric Measurement Techniques*, 11(1), 215–232. https://doi.org/10.5194/amt-11-215-2018
- Preusse, P., Eckermann, S. D., Ern, M., Oberheide, J., Picard, R. H., Roble, R. G., et al. (2009). Global ray tracing simulations of the SABER gravity wave climatology. *Journal of Geophysical Research*, 114, D08126. https://doi.org/10.1029/2008JD011214
- Preusse, P., Ern, M., Bechtold, P., Eckermann, S. D., Kalisch, S., Trinh, Q. T., & Riese, M. (2014). Characteristics of gravity waves resolved by ECMWF. Atmospheric Chemistry and Physics, 14(19), 10483–10508. https://doi.org/10.5194/acp-14-10483-2014
- Preusse, P., Ern, M., Eckermann, S. D., Warner, C. D., Picard, R. H., Knieling, P., et al. (2006). Tropopause to mesopause gravity waves in august: Measurement and modeling. *Journal of Atmospheric and Solar-Terrestrial Physics*, 68(15), 1730–1751. https://doi.org/10.1016/j.iastp.2005.10.019
- Pulido, M., Rodas, C., Dechat, D., & Lucini, M. M. (2013). High gravity-wave activity observed in Patagonia, southern America: Generation by a cyclone passage over the Andes mountain range. *Quarterly Journal of the Royal Meteorological Society*, 139, 451–466.
- Sato, K., Tateno, S., Watanabe, S., & Kawatani, Y. (2012). Gravity wave characteristics in the southern hemisphere revealed by a high-resolution middle-atmosphere general circulation model. *Journal of the Atmospheric Sciences*, 69(4), 1378–1396. https://doi.org/10.1175/jas-d-11-0101.1
- Stockwell, R., Mansinha, L., & Lowe, R. (1996). Localization of the complex spectrum: The s transform. *IEEE Transactions on Signal Processing*, 44(4), 998–1001.
- Vosper, S. B. (2015). Mountain waves and wakes generated by south Georgia: Implications for drag parametrization. Quarterly Journal of the Royal Meteorological Society, 141(692), 2813–2827.
- Wells, H., Vosper, S. B., & Yan, X. (2011). An assessment of a mountain-wave parametrization scheme using satellite observations of stratospheric gravity waves. *Quarterly Journal of the Royal Meteorological Society*, 137, 819–828.
- Wright, C. J., & Gille, J. C. (2013). Detecting overlapping gravity waves using the s-transform. *Geophysical Research Letters*, 40, 1850–1855. https://doi.org/10.1002/grl.50378
- Wright, C. J., & Hindley, N. P. (2018). How well do stratospheric reanalyzes reproduce high-resolution satellite temperature measurements?. Atmospheric Chemistry and Physics, 18(18), 13703–13731.
- Wright, C. J., Hindley, N. P., Hoffmann, L., Alexander, M. J., & Mitchell, N. J. (2017). Exploring gravity wave characteristics in 3-d using a novel s-transform technique: AIRS/aqua measurements over the southern andes and drake passage. *Atmospheric Chemistry and Physics*, 17(13), 8553–8575.
- Wright, C. J., Hindley, N. P., & Mitchell, N. J. (2016). Combining AIRS and MLS observations for three-dimensional gravity wave measurement. *Geophysical Research Letters*, 43, 884–893. https://doi.org/10.1002/2015GL067233
- Zhong, L., Sonmor, L. J., Manson, A. H., & Meek, C. E. (1995). The influence of time-dependent wind on gravity-wave propagation in the middle atmosphere. *Annales Geophysicae*, 13(4), 375–394. https://doi.org/10.1007/s00585-995-0375-6

PERRETT ET AL. 10 of 10